ROYAL SOCIETY
OF CHEMISTRY

PAPER

Prospective life cycle assessment of organic redox flow batteries†

Shan Zhang, [iD] *[a] Athul Seshadri Ramanujam,[b,c,d] Rickard Arvidsson, [iD] [e]
Alessandro Michieletto[f,g] and Ulrich S. Schubert [iD] [f,g,h]

Redox flow batteries (RFBs) are considered a promising technology for stationary energy storage. Organic redox flow batteries (OFBs) are emerging as alternatives to vanadium redox flow batteries (VFBs), since the former consist of cheap and abundant organic materials with the potential to offer lower environmental impacts. Despite numerous life cycle assessment (LCA) studies of VFBs, there is a lack of LCAs of OFBs. In this study, this gap is addressed by an LCA of an OFB and a hybrid redox flow battery (HFB) based on TEMPO electrolytes. A battery design model and a battery performance model were established to provide part of the inventory data required for the LCA. Compared to VFBs, OFBs and HFBs demonstrated superior cradle-to-gate environmental performance for acidification, human toxicity (carcinogenic), and particulate matter, but inferior performance for climate impact, freshwater ecotoxicity, and resource depletion. The primary environmental hotspots associated with battery production were electrolyte active materials, inverters, and end plates. The cradle-to-use environmental impact results showed that the OFB outperformed the VFB and HFB, primarily because the OFB's low electrolyte capacity fade rate leads to reduced electrolyte consumption during use. Sensitivity analysis indicates that future research should prioritize improvements to the electrolyte capacity fade rate. Given the early development stage of OFB and HFB technologies, there is potential to improve them further into more environmentally friendly energy storage systems.

Broader context

To support the European Commission's green deal objectives, decarbonizing electricity sources is essential, with an emphasis on integrating renewable energies. This transition drives the development of safe, cost-effective stationary electrochemical energy storage systems. Among these, organic electrolyte-based redox flow batteries are attracting attention from researchers and industry as a promising solution. Despite their potential, the environmental impacts of these technologies remain inadequately addressed. This study conducts a comprehensive environmental assessment of two redox flow batteries with TEMPO-based electrolytes using life cycle assessment (LCA). We developed a battery design model based on industrial equations and a performance model that accounts for electrolyte degradation during the use phase. Furthermore, uncertainty and sensitivity analyses identify the most influential battery performance parameters affecting the LCA results. Redox flow batteries with TEMPO-based electrolytes are found to be promising in cradle-to-use LCA results. The findings also identify opportunities to improve environmental performance by reducing electrolyte capacity fade. The results serve as benchmarks for future research and support ongoing efforts to reduce the environmental footprint of organic redox flow batteries.

[a]Department of Energy and Technology, Swedish University of Agricultural Sciences, P.O Box 7032, SE-75007 Uppsala, Sweden. E-mail: shan.zhang@chalmers.se
[b]Electrochemical Processes Unit, IMDEA Energy, Avda. Ramón de la Sagra 3, 28935 Móstoles, Spain
[c]Energy Storage Solutions E22, Avenida de Barajas 32, Parque Empresarial Omega Edificio A, 28108 Alcobendas, Spain
[d]Department of Applied Chemistry, Faculty of Science, University of the Basque Country UPV/EHU, Avda. Manuel de Lardizabal 3, 20018 Donostia-San Sebastián, Spain

[e]Division of Environmental Systems Analysis, Department of Technology Management and Economics, Chalmers University of Technology, Gothenburg 41296, Sweden
[f]Laboratory of Organic and Macromolecular Chemistry (IOMC), Friedrich Schiller University Jena, Humboldtstraße 10, 07743 Jena, Germany
[g]Center for Energy and Environmental Chemistry Jena (CEEC Jena), Friedrich Schiller University Jena, Philosophenweg 7a, Jena 07743, Germany
[h]Helmholtz Institute for Polymers in Energy Applications (HIPOLE Jena), Lessingstrasse 12-14, Jena 07743, Germany
†Electronic supplementary information (ESI) available. See DOI: https://doi.org/10.1039/d4eb00027g

1. Introduction

Society undergoes a rapid energy transition from the use of fossil fuels to renewable energy sources, such as wind and solar power. Based on current policies and market development, the International Energy Agency (IEA) predicts that renewables will be the largest electricity source globally by 2025, accounting for over 90% of global electricity capacity expansion.[1] Bogdanov *et al.* (2019) suggested that solar photovoltaics (PV) and wind are going to be the main electricity generation technologies to achieve a 100% renewable electricity system by 2050.[2] However, the intermittent nature of these renewable energy sources poses a challenge for maintaining a stable and uninterrupted electricity supply.[3] Moreover, the demand to reduce electricity costs and the availability of government incentives for solar and battery storage systems are driving the rapid development of residential battery energy storage systems.[4–6] For instance, in Germany and Italy, over 70% of home solar systems now include batteries, significantly reducing the need for grid upgrades.[4] This highlights the importance of residential-scale energy storage solutions in optimizing the use of renewable energy technologies. Redox flow batteries (RFBs) constitute a potential solution for stationary and household energy storage because of their unique ability to tailor power and energy separately, coupled with their prolonged lifespan, minimal self-discharge, and robust safety features.[7,8] Among the range of RFBs, the vanadium redox flow battery (VFB) is a well-established type that has been commercially utilized for several decades.[7] Despite its high level of maturity, the widespread adoption of VFBs is constrained by high upfront costs and the volatile supply of vanadium.[9–11] These challenges have encouraged researchers to investigate new charge-storage materials based on abundant elements, such as organic compounds. Reflecting this shift, several companies, including CMBlu, Kemiwatt, Redflow, and e-Zinc, are now actively working to commercialize organic flow batteries (OFBs) and hybrid flow batteries (HFBs).

Among different organic components, anthraquinone (AQ) derivatives, 2,2,6,6-tetramethylpiperidine-1-oxyl (TEMPO) based organic molecules, and viologens have been widely explored as promising energy storage materials. AQ derivatives features with their reversible two-electron redox reaction (AQ/ AQ^-/AQ^{2-}), high chemical stability, and large molecular structure that can suppress crossover.[12] AQ derivatives often perform effectively in acidic or alkaline conditions,[13–16] and significant research efforts have been made to develop AQ derivatives stable in neutral pH environment.[13,17,18] TEMPO-based organic materials have also attracted significant attention as electrolyte candidate for RFBs.[13,19,20] TEMPO-based nitroxide radicals and viologen are particularly promising pairs for RFB applications, as they can operate effectively at neutral pH, achieve high concentrations, and deliver relatively high potentials in aqueous solutions, bringing TEMPO/viologen systems closer to industrial implementation.[9,10,13]

Given the increasing interest in TEMPO-based RFBs, environmental assessment studies on such systems remain limited. To date, most life cycle assessment (LCA) studies have focused on VFBs,[21–25] with one study assessing an AQ-based HFB[26] and another evaluating TEMPO-based OFB.[27] Moreover, data for battery composition and performance are often derived from simplified estimations. This study aims to evaluate the environmental performance of two emerging TEMPO-based RFBs: an all-organic redox flow battery (OFB) and a hybrid redox flow battery (HFB), using LCA combined with battery design and performance models. The battery design and performance model was developed under the assumption that these two emerging batteries are already being produced at an industrial scale. Additionally, this study aims to identify key battery performance parameters that contribute to uncertainties in the environmental impact results. The environmental performance of OFB and HFB was benchmarked against VFBs. These results can help guide flow battery developers and companies in improving the environmental performance of these technologies and serve as a benchmark for future LCA studies of OFBs.

2. Materials and methods

The methodological framework, as depicted in Fig. 1, consists of three core components: (i) a battery design model (green dashed-line box), (ii) a battery performance model (blue dashed-line box), and (iii) a LCA model (purple dashed-line box). The outputs of the battery design model (dark green box) and the battery performance model (dark blue boxes) serve as inputs for the LCA model. Various parameters (yellow boxes) are required as inputs for these models. Subsequently, a LCA is performed to quantify the environmental impacts of the three studied RFBs (OFB, HFB and VFB). This section is structured as follows: the battery technology is first described (section 2.1), followed by the battery performance (section 2.2), and the LCA phases (section 2.3). This study includes the four key LCA phases: goal and scope definition (section 2.3.1), life cycle inventory analysis (LCI) (section 2.3.2), life cycle impact assessment (LCIA) (section 2.3.3), and interpretation (section 2.3.4). As part of the interpretation, an uncertainty analysis (UA) and sensitivity analysis (SA) are performed to quantify uncertainty in the model's results and to identify the battery performance-related parameters that contribute the most to it[28] (yellow boxes with bold black texts).

2.1 Redox flow battery design

This study developed a RFB design model to calculate the amounts of battery materials required for each component, ensuring a fair comparison between the three studied RFB types. The RFBs were designed with a power rating of 5 kW and a theoretical capacity of 40 kW h (*i.e.*, an energy-power ratio of 8 : 1). The intended application was a residential energy storage connected to rooftop solar systems. The RFBs comprise three main parts: a power subsystem (cell stack), an energy subsystem including electrolytes and container tanks, and a periphery with ancillary components (Fig. 2). The elec-
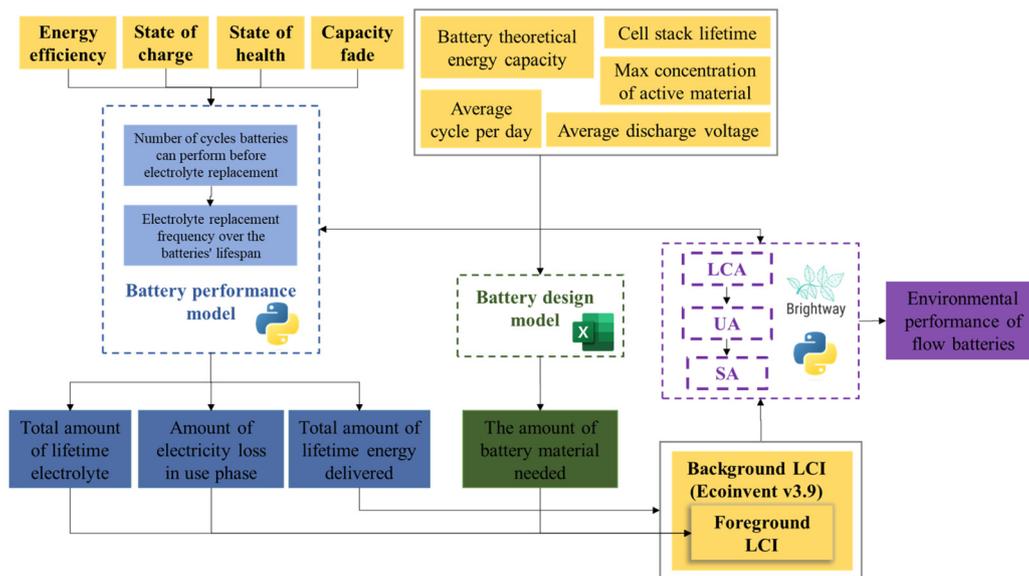
Fig. 1 Methodological framework schematic. Yellow boxes denote input data for sub-models, with those featuring bold black text signifying parameters included in the SA. Blue, green, and purple dashed-line boxes correspond to the battery performance model, battery design model, and LCA model, respectively. Dark blue, dark green and dark purple boxes represent the respective model outputs.
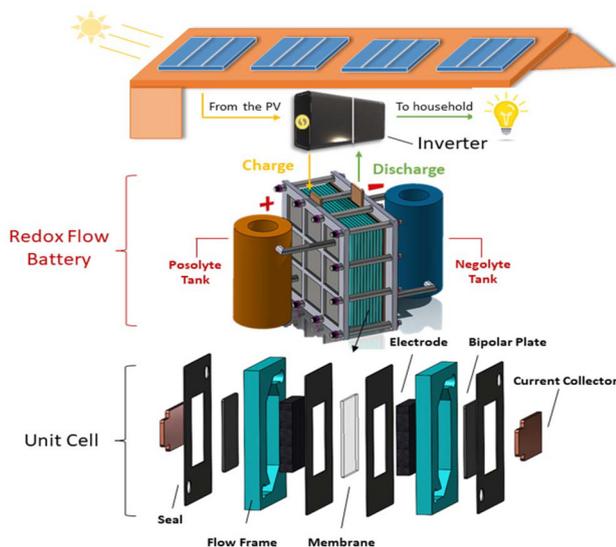

Fig. 2 Schematic representation of a RFB stack and a conventional laboratory-scale breakdown of unit cell.

trolytes stored in the tanks differ in terms of both the dissolved active materials and redox potentials. The electrolyte passing through the positive electrode is called posolyte, while the electrolyte passing through the negative electrode is called negolyte.

The power subsystem consists of a single stack of unit cells connected in series. The number of unit cells and electrode sizes were determined based on rated power, discharge voltage, and current densities. Relevant data for the VFB were provided by the company Energy Storage Solutions S.L. (E22),

while data for the OFB and HFB were collected from the literature, considering factors such as solubility of active species, operable current density, and long-term cycling stability.[19,29] For example, different electrolyte concentrations were selected for the three studied flow battery systems based on values reported in long-term cyclability tests, as these concentrations represent the optimal balance between maximizing battery capacity and ensuring stable operation over extended cycles. Each unit cell includes an ion-exchange membrane, two graphite felt electrodes, two bipolar plates made of carbon-composite material serving as the contact between two cells in series, two copper current collectors acting as battery terminals, a plastic flow frame directing the electrolyte towards the felt, and two end plates compressing and sealing all battery components together. Details of the compositions are presented in Table 1.

In operation, RFBs function in two modes: charging, where they receive electricity from the PV panels, and discharging, where they supply electricity. An inverter converts the direct current (DC) produced by the cell stack into alternating current (AC) for households and *vice versa*. Negolyte and posolyte stored in container tanks are pumped through the stack, generating a potential difference between the membrane, which enables ion exchange but prevents electrolyte mixing.

Membrane, bipolar plate, and current collector areas were designed to be 20%, 10%, and 10% larger than the electrode area, respectively.[30] Such design promotes optimal contact between the components and minimize electrolyte leakage.[30,31] Additionally, electrolyte tanks were sized slightly larger than the electrolyte volume, with inert gas filling the surplus volume to prevent atmospheric oxygen contamination.[32] The technical data and final battery compositions (in

Table 1 Compositions of the studied RFBs

Component	VFB	OFB	HFB
Power subsystem (cell stack)			
Membrane	Nafion 212	Fumasep FAA-3-PE-30	Fumasep F-930-RFD
Bipolar plates	Graphite		
Electrodes	Graphite felt	Graphite felt	Graphite felt & zinc foil
Current collector	Copper		
Flow frames/current collector housing	Polypropylene		
End plates	Aluminium		
Seals	FKM rubber		
Screws	Steel		
Energy subsystem			
Negolyte active material	0.9 M V_2O_5	2 M MV	2 M $ZnCl_2$
Posolyte active material	0.9 M V_2O_5	2 M TEMPTMA	1 M TEMPO-4-SO_3K
Solvent	H_2O		
Additive 1	0.05 M H_3PO_4	0.3 M NaCl	1 M NH_4Cl
Additive 2	2.1 M H_2SO_4	—	2 M $ZnCl_2$
Tank	HDPE		
Periphery			
Pipes	Polyvinyl chloride		
Pumps	Cast iron & steel		
Inverters	Aluminium, copper, steel, polypropylene		
Electrical cables	Copper		

MV = methyl viologen or *N,N*-dimethyl-4,4-bipyridinium dichloride. TEMPTMA = *N,N,N*-2,2,6,6-heptamethylpiperidinyl oxy-4-ammonium chloride. TEMPO-4-SO_3K = 2,2,6,6-tetramethylpiperidone-4-sulfate potassium.

Table 2 Technical data for the studied RFBs

Technical parameters	VFB	OFB	HFB
Power (kW)	5	5	5
Theoretical capacity (kW h)	40	40	40
Energy density (W h kg^{-1})	27	16	15
Discharge voltage per cell (V)	1	1	1.25
Number of cells	13	13	11
Weight (kg)	1476	2470	2616

wt%) are presented in Table 2 and Fig. 3, respectively. The model equations used for calculating battery dimensions are from company E22, which cannot be presented for confidentiality reasons. The additional battery dimension results can be found in the ESI 1 (section S1†).

2.2 Redox flow battery performance

The battery performance parameters can affect the total electricity delivered throughout the operational lifespan of the RFB, the electrolyte replacement frequency, and the electricity required during use. These factors could, in turn, influence the environmental impacts of RFBs. Battery performance parameters considered in this study are the energy efficiency (EE), operating state-of-charge range (ΔSoC), state-of-health (SOH_{limit}), and electrolyte degradation, specifically in terms of capacity fade per cycle (CF).[3] EE in this study refers to the net round-trip efficiency, including the efficiency of power consumption of pumps, inverter, and transformer.[33] ΔSoC refers to the ratio of its charged capacity each cycle to its theoretical capacity. SOH_{limit} represents the minimum allowable capacity relative to the original capacity, indicating the end-of-life (EoL) of electrolytes. The estimated value of each parameter for the studied RFBs and their respective probability density functions (PDFs) used in the sensitivity analysis were summarized in Tables 3 and 4. The most likely value in the PERT distribution was used as the estimated parameter value. High-performance laboratory data were used to estimate the potential performance that flow batteries could achieve at an industrial scale.
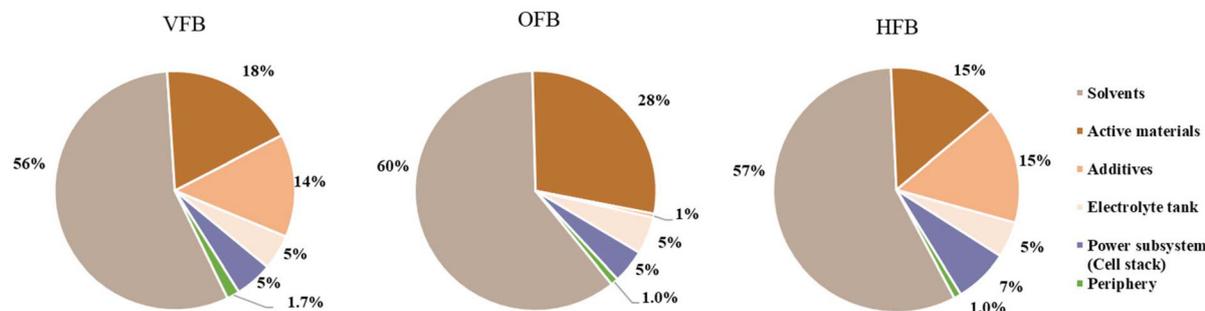

Fig. 3 Composition (in wt%) of three studied RFBs.

Table 3 Estimated battery performance parameter values for three RFBs

Parameters	VFB	OFB	HFB
Energy efficiency (%)	80	73	70
Operating state-of-charge range (%)	70	90	100
State of health (%)	73	73	73
Capacity fade (% per cycle)	0.07	0.037	0.085

References used to determine the parameter values can be found in the ESI 1 (section S2.2†).

It was assumed in the battery performance model that the electrolyte tank, cell stack and peripheral components have a duration of 20 years for the three studied RFBs. This aligns with assumptions used in previous studies.[21,22,34] Energy arbitrage using battery storage system usually assumes a daily cycling rate of around 1.[35] An average daily cycling rate (n) of 1.12 cycles was expected for the three studied RFBs.[36,37] Furthermore, it was assumed that each cycle leads to a specific degree of capacity fade in the electrolyte. Consequently, the electrolyte will be replaced when it reaches the predefined SoH$_{limit}$. This replacement practice continues until other battery components reach their EoL, *i.e.* after 20 years.

With the predefined cell stack lifetime L_{stack} and the average daily cycling rate n, the electrolyte replacement frequency (N) though the RFB's lifetime can be calculated as:

$$N = \frac{L_{stack} \times 365 \times n}{l_{cyc}} - 1 \quad (1)$$

Note that the results for N were rounded up to the next integer for decimal values. l_{cyc} is the number of cycles a RFB can perform without significant capacity loss or the number of cycles a RFB can reach before the electrolyte replacement, which can be calculated as:

$$(1 - q)^{l_{cyc}} \geq SOH_{limit} \quad (2)$$

where q is the predefined capacity fade, which refers to a percentage of capacity lost by the electrolyte per cycle. SOH$_{limit}$ refers to the predefined state-of-health limit for electrolyte replacement. The total amount of electrolyte needed throughout battery's lifetime can be calculated by multiplying ($N + 1$) with the amount of electrolyte required for one flow cell.

The cell stack and the periphery parts will reach their EoL at the same time or before the electrolytes reached their SOH$_{limit}$ in the last electrolyte replacement round. Therefore, the number of cycles a RFB can perform after the last electrolyte replacement $l_{cyc,last}$ is less than or equal to l_{cyc}, which can be calculated as:

$$l_{cyc,last} = L_{stack} \times 365 \times n - l_{cyc} \times N \quad (3)$$

The total amount of energy that can be expected from a RFB over its lifespan ($W_{B,total}$) can be calculated as:

$$W_{B,total} = W_{B,l_{cyc}} \times N + W_{B,l_{cyc,last}} \quad (4)$$

where $W_{B,l_{cyc}}$ refers to the amount of energy a RFB can deliver before electrolyte replacement, $W_{B,l_{cyc,last}}$ refers to the amount of energy a RFB can deliver after the last electrolyte replacement. These two variables can be calculated as:

$$W_{B,l_{cyc}} = W_1 + W_2 + W_3 + \ldots + W_{l_{cyc}} = \sum_{i=1}^{l_{cyc}} W_i = \sum_{i=1}^{l_{cyc}} W_B^0 (1 - q)^i \quad (5)$$

$$W_{B,l_{cyc,last}} = W_1 + W_2 + W_3 + \ldots + W_{l_{cyc,last}} = \sum_{i=1}^{l_{cyc,last}} W_i$$
$$= \sum_{i=1}^{l_{cyc,last}} W_B^0 (1 - q)^i \quad (6)$$

W_B^0 refers to the nominal capacity at the first charge–discharge cycle, which can be calculated as:

$$W_B^0 = \text{theoretical battery capacity} \times \Delta SoC \times EE = 40 \, kW \, h \times \Delta SoC \times \eta_{EE} \quad (7)$$

ΔSoC and η_{EE} are the percentage of the capacity that the battery can deliver in each charging cycle and energy efficiency, respectively, of which the latter is calculated as:

$$\eta_{EE} = \frac{\text{electricity delivered}}{\text{electrcity consumed}}$$
$$= \frac{\text{electricity delivered}}{\text{electricity delivered} + \text{electricity loss}}. \quad (8)$$

2.3 Life cycle assessment

2.3.1 Goal and scope definition. The goal of the study was to conduct a comparative life cycle assessment of three types of RFBs: an OFB, a HFB, and a VFB. Given the relatively low technology readiness level (TRL) of the OFB and HFB (TRL = ~4) and the lack of comprehensive data on their performance,

Table 4 Probability density functions of battery performance parameters for three RFBs

Parameters	VFB	OFB	HFB
Energy efficiency	Uniform (min: 50%, max: 90%)	Uniform (min: 50%, max: 90%)	Uniform (min: 50%, max: 90%)
Operating state-of-charge range	PERT (min: 60%, mode: 70%, max: 100%)	PERT (min: 60%, mode: 90%, max: 100%)	PERT (min: 60%, mode: 100%, max: 100%)
State of health	PERT (min: 65%, mode: 73%, max: 80%)	PERT (min: 65%, mode: 73%, max: 80%)	PERT (min: 65%, mode: 73%, max: 80%)
Capacity fade	PERT (min: 0%, mode: 0.07%, max: 0.1%)	PERT (min: 0%, mode: 0.037%, max: 0.1%)	PERT (min: 0%, mode: 0.085%, max: 0.1%)

© 2025 The Author(s). Published by the Royal Society of Chemistry

considerable uncertainties were associated with the battery use phase. However, quantifying the influence of performance parameters, including the battery use phase, on the environmental performance of energy storage technologies[38,39] can provide a more comprehensive understanding. Therefore, two functional units (FU) were included in this study: FU1 was 1 kW h theoretical storage capacity with a cradle-to-gate system boundary, and FU2 was 1 kW h electricity delivered over battery lifetime with a cradle-to-use system boundary. This approach with two FUs with different system boundaries has also been applied by.[40] End-of-life (EoL) was not considered because of the high uncertainty related to the recycling technology for TEMPO-based electrolyte used in the OFB and the HFB.

As presented in eqn (9), the total impact for environmental category c with FU1 was calculated as the sum of the life cycle environmental impact scores (IS) associated with the RFB production, divided by the theoretical storage capacity. The total impact for environmental category c with FU2 was calculated as the sum of IS associated with battery production, electrolyte replacement and electricity losses in the use phase, divided by the lifetime electricity delivered by the RFBs ($W_{B,total}$) (eqn (10) and (11)).

$$IS_{c,FU1} = \frac{IS_{c,\text{power subsystem}} + IS_{c,\text{energy subsystem}} + IS_{c,\text{periphery subsystem}}}{\text{theoretical storage capacity}}$$

(9)

$$IS_{c,FU2} = \frac{(IS_{c,\text{power subsystem}} + IS_{c,\text{energy subsystem}} + IS_{c,\text{periphery subsystem}}) + IS_{c,\text{use phase}}}{W_{B,total}}$$

(10)

$$IS_{c,\text{use phase}} = IS_{c,\text{electricity loss}} + IS_{c,\text{electrolyte replacement}}$$

(11)

The electricity used to power RFBs were from solar panels. Other electricity consumed in the foreground was the average European electricity mixture. Based on the time it took for the first generation of lithium-ion batteries to go from innovation to the market,[41] and considering the fast development in battery technology, we estimated that the OFBs and HFBs could reach the highest TRL (i.e., 9) in the next decade, e.g., 2030–2035. The LCA was calculated using Brightway.[42]

2.3.2 Life cycle inventory analysis. For the production of battery materials, the Ecoinvent database 3.9 (cut-off) and previous LCA studies were used whenever feasible. The LCI for V_2O_5 as an electrolyte active material was obtained from ref. 23, and the LCI for the inverter from ref. 43. Due to the emergence of OFBs, LCI data for certain battery materials were unavailable. To address this, we developed our own LCI by identifying production routes based on patent and literature sources, supplemented by auxiliary inputs (e.g., energy, inert gas, and cooling water) calculated using empirical parameters reported from prior studies.[44–46]

The negolyte active material for the OFB, MV, was modelled using a LCI for bipyridylium-compound production (RER) from Ecoinvent 3.9. The LCI for the posolyte active materials of the OFBs and HFBs was established based on the production chain illustrated in Fig. 4. Initially, triacetone amine (TAA), a precursor for both posolyte active materials, was synthesized through the reaction of acetone and ammonia.[47] For TEMPTMA, the posolyte active material of the OFB, production processes described by ref. 48 were followed: TAA was reacted with dimethylamine to yield 4-dimethylamino-2,6,6-etramethylpiperidine (intermediate 1). Intermediate 1 then reacted with chloromethane to form N,N,N-2,6,6-heptamethyl-piperidin-4-ammonium chloride (intermediate 2). Subsequently, TEMPTMA was produced by reacting intermediate 2 with H_2O_2. To prepare the posolyte active material of the HFB, TEMPO-4-SO_3K, TAA was first reduced by H_2 to form 4-hydroxy-TEMP.[49] Following this, 4-hydroxy-TEMPO was synthesized through the reaction with EDTA disodium salt dehydrate.[50] Finally, TEMPO-4-SO_3K was produced by reacting 4-hydroxy-TEMPO with concentrated sulfuric acid and $KHCO_3$.[29] Detailed descriptions of unit processes and energy
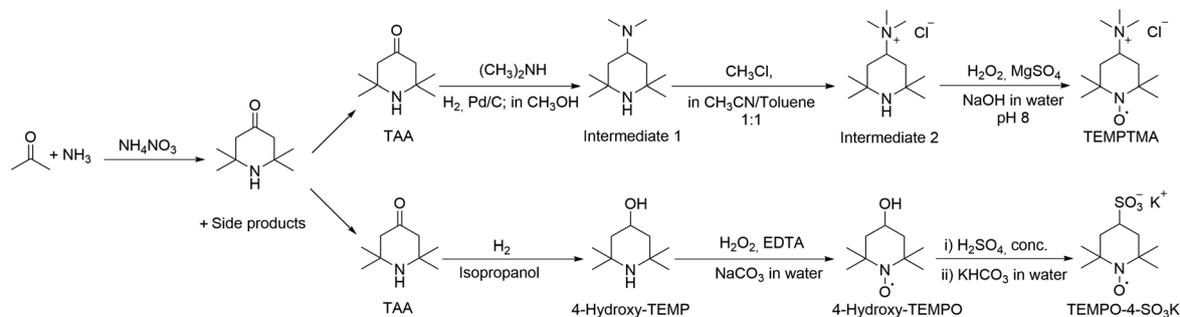

Fig. 4 Production process of electrolyte active materials. Intermediate 1 refers to 4-dimethylamino-2,2,6,6-etramethylpiperidine. Intermediate 2 refers to N,N,N-2,2,6,6-heptamethylpiperidin-4-ammonium chloride. 4-Hydroxy-TEMPO refers to 4-hydroxy-2,2,6,6-tetramethylpiperidine-N-oxyl. 4-Hydroxy-TEMP refers to 4-hydroxy-2,2,6,6-tetramethylpiperidine. TAA refers to 2,2,6,6-tetramethyl-4-piperidone/triacetone amine.

consumption calculations are provided in ESI 1 (section S2), with the full inventory available in ESI 2.†

2.3.3 Life cycle impact assessment. The environmental footprint (EF v3.1) midpoint method was used to calculate the environmental impact scores, focusing on six key impact categories: acidification, climate change, freshwater ecotoxicity, human toxicity (carcinogenic), resource depletion, and particulate matter formation. These categories were selected because flow battery production involves metals and organic solvents, which significantly contribute to these impacts. For instance, metal extraction affects climate change, acidification, toxicity, particulate matter, and resource depletion, while organic solvent production is linked to climate change and toxicity.[51] These categories are also selected as significant in other LCAs on flow batteries.[52] Additional impact category results are available in the ESI 1 (section S3†).

2.3.4 Interpretation. This step presents the environmental performance of the OFB and HFB in comparison to the VFB. First, a comparative analysis of the environmental impacts of VFB, OFB, and HFB was performed for the six impact categories and the two FUs. Next, the hotspots of each battery were outlined, with a focus on OFB and HFB. Subsequently, an uncertainty analysis was conducted to quantify uncertainty in the impact scores using Monte Carlo simulation. Finally, a SA was conducted to reveal the most influential battery performance parameters, considering the uncertainties related to battery performance parameters.

The uncertainty analysis started by generating 1000 samples for each battery performance parameter based on their respective PDFs. These randomly generated samples were input into the battery performance model to produce intermediate parameters. These intermediate parameters were subsequently used in the LCA model to run Monte Carlos simulation, as implemented by the Python package presamples, to compute 1000 times of LCA using Brightway. The delta moment independent method proposed by Borgonovo[53,54] was employed to evaluate the influence of battery performance parameters on the corresponding LCA results, using Python package SALib.[55] The delta moment independent method quantifies the influence of a model's input uncertainties on the output uncertainty, taking into account the interactions between inputs. Unlike one-at-a-time (OAT) approaches, which vary one parameter at a time while keeping all other parameters constant, the delta method provides a more thorough analysis by allowing parameters to vary across their full distributions.[56] Compared to other SA methods, such as Sobol method, delta method considers the uncertainties in input parameters on the entire distribution shape, rather than just on moments like variance.

3. Results and interpretation

3.1 Cradle-to-gate impacts

Fig. 5(a) displays the comparison of three studied RFBs using a FU of 1 kW h of theoretical storage capacity. Despite the significantly lower TRL of the OFB and HFB, they demonstrate lower impacts compared to the commercially available VFB for several impact categories. Fig. 5(b) presents the relative contribution of battery components. Overall, the energy subsystem, comprising the negolyte and posolyte active materials, additives, and electrolyte tank, is the primary contributor (58 to 96% of the total impacts) for three studied RFBs in most of the impact categories except resource depletion (11 to 51% of the total impact). This can be attributed to the high per-kg environmental impacts of the electrolyte active materials, as well as the relatively large quantities of electrolyte active materials used in the RFBs (15 to 28% of total weight, Fig. 3). While solvents (deionized water) account for 56 to 60% of the total weight of RFBs, their impacts were not considered in the analysis due to their negligible contributions (<0.1%).

3.1.1 Acidification. HFB exhibits the most favorable performance (1.01 mol H+-Eq), followed by OFB (2.03 mol H+-Eq) and VFB (3.91 mol H+-Eq). In the case of OFB, 65% of the acidification comes from the production of the negolyte active material MV, with 39% directly attributed to the unit process emissions from MV production and 26% stemming from upstream production processes. The direct impact from the production of MV is caused by the emissions of ammonia, nitrogen oxides, sulfur dioxide, and sulfur trioxide. Approximately 19% of the impact is associated with the production of the posolyte active material TEMPTMA. The production of MV and TEMPTMA involves the use of significant quantities and a variety of raw materials, resulting in a high energy demand. The energy production processes lead to emissions of sulfur and nitrogen oxides, contributing to the high acidification impact. The periphery components account for 9% of the acidification impact, primarily due to inverter production (8%). The cell stack contributes approximately 6% to the overall acidification.

In the HFB, the posolyte active material, TEMPO-4-SO$_3$K, is the largest contributor, accounting for 40% of the total impact. This primarily stems from the production of 4-hydroxy-TEMPO (Fig. 4), which alone accounts for 24% of the total impact. Additional contributing chemicals include ethyl acetate (6%), sulfuric acid (4%), and acetone (2%). The cell stack (20%) is another key contributor, primarily due to the use of aluminium (13%) as the end plate material. Periphery components account for 19% to the impact, with the inverter circuit being the major factor, responsible for this high contribution (16%). ZnCl$_2$, serving as both the negolyte active material and additive, accounts for 15% of the acidification. Due to the relatively lower acidification contribution from electrolyte active materials, the cell stack and periphery components of the HFB exhibit relatively higher contribution as compared to the OFB.

3.1.2 Climate change. The VFB demonstrates the best climate impact performance (193 kg CO$_2$-Eq), followed closely by the HFB (212 kg CO$_2$-Eq) and the OFB (274 kg CO$_2$-Eq). For the OFB, the posolyte active material TEMPTMA stands out as the biggest contributor, accounting for 51% of the climate change impact. This can be attributed to the extensive pro-
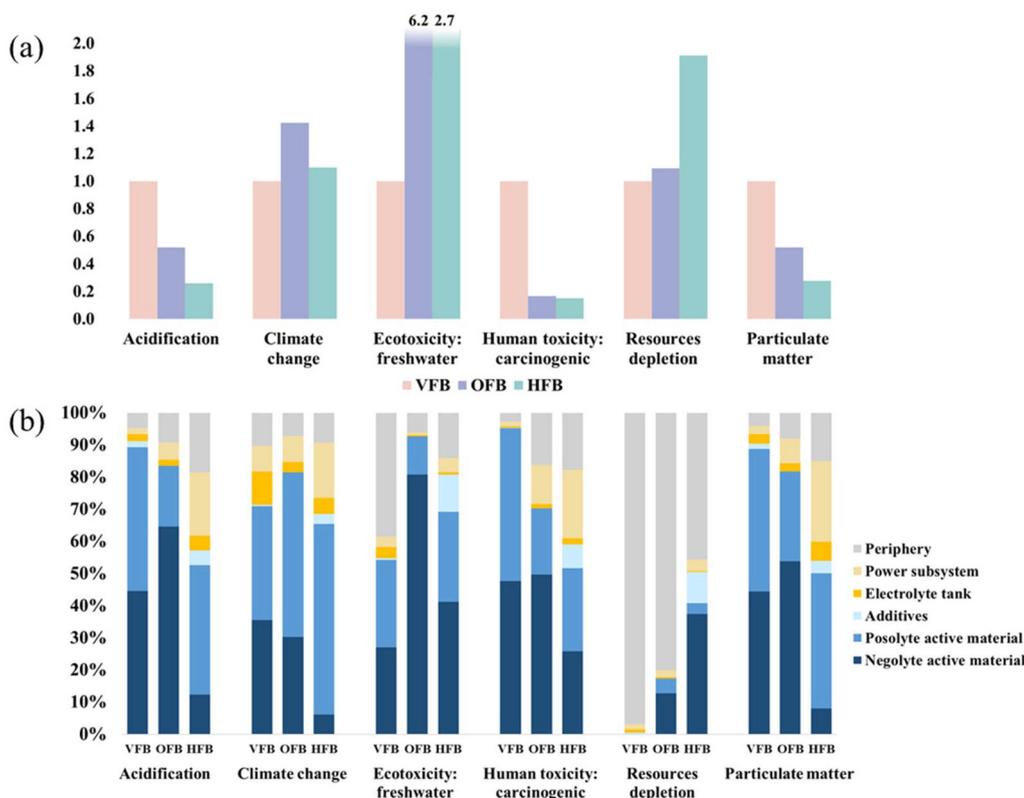
Fig. 5 (a) Comparative environmental impacts of three RFBs, with a functional unit (FU1) of 1 kW h storage capacity. The impacts of VRB are set to 1.0 for comparison. (b) Breakdown of the environmental impacts from manufacturing the three RFBs to battery components, with a FU of 1 kW h energy storage capacity. VFB = vanadium redox flow battery, OFB = organic redox flow battery, HFB = hybrid redox flow battery.

duction chain of TEMPTMA, characterized by high energy consumption and substantial waste generation, leading to high greenhouse gas (GHG) emissions. MV (30%) is another substantial contributor, primarily due to the high raw material requirements in MV production, resulting in notable GHG emissions. The cell stack (8%) also makes a notable contribution, with its climate impact attributed to various components, including end plates (4%), cell frames (2%), and seals (2%). Periphery components contribute 7% to the climate impact, primarily due to the inverter production.

In the case of HFB, 59% of the impact can be attributed to the posolyte active material TEMPO-4-SO$_3$K, driven by the high energy consumption (*e.g.*, steam, heat, electricity) and the generation of substantial waste requiring treatment throughout the production chain. Additionally, 17% of the impact is associated with the cell stack, with 9% stemming from end plates, 4% from cell flow frames, and 3% from seals. Production of ZnCl$_2$ accounts for approximately 8% of the climate change impact. Periphery components contribute 9% to the climate impact, with the inverter being the primary contributor.

3.1.3 Freshwater ecotoxicity. The OFB (9318 CTUe) and the HFB (4085 CTUe) exhibit notably higher impact scores compared to the VFB (1497 CTUe), representing approximately 6 and 3 times the impact of the VFB, respectively. The high

freshwater ecotoxicity caused by the OFB production is primarily caused by the MV production processes, accounting for 81% of the impact. Within this, 68% originates directly from the MV production process, with an additional 13% associated with upstream processes. The production of MV results in substantial emissions of chloride and chloroacetic acid, further contributing to significant freshwater ecotoxicity. Another notable contributor is the production of TEMPTMA, which accounts for 12% of the freshwater ecotoxicity. Additionally, periphery components also play a substantial role (6%), which is caused by the production of circuits used in the inverter.

For the HFB, the high freshwater ecotoxicity results can predominantly be traced to the use of ZnCl$_2$ (52%) as both the negolyte active material and electrolyte additive. This impact can be linked to upstream processes associated with mining, processing and refining of the element zinc (51%), resulting in considerable emissions of hydrogen sulfide that impacts aquatic ecosystems. The use of TEMPO-4-SO$_3$K (28%) as the posolyte material represents another major contributor, primarily due to the use of potassium bicarbonate as a raw material, as well as the related waste treatment processes. The periphery components account for 14% of the freshwater ecotoxicity, while the cell stack contributes 4%.

3.1.4 Human toxicity (carcinogenic). The HFB (2.6×10^{-7} CTUh) results in best performance for human toxicity (carcino-

genic), followed by the OFB (2.9×10^{-7} CTUh) and the VFB (1.7×10^{-6} CTUh). In the OFB, the MV stands out as the most substantial contributor, accounting for 50% of the carcinogenic toxicity impact, with 7% directly attributable to the MV production and 43% stemming from upstream processes. TEMPTMA contributes 21% to the impact, while the periphery components account for 16%, primarily due to the usage of pumps (7%) and inverters (8%). The cell stack contributes 12% of the human toxicity (carcinogenic), with components such as end plates (5%) and screws (4%) are identified as notable additional sub-contributors.

For the HFB, $ZnCl_2$ emerges as the largest contributor, making up 32% of the human toxicity (carcinogenic). This dominance is mainly attributed to toxic emissions during zinc mining operations. The posolyte material TEMPO-4-SO_3K follows as the second most significant contributor, accounting for 26% of the human toxicity (carcinogenic), followed by the cell stack (21%), and the periphery components (18%).

3.1.5 Resource depletion. The HFB (16 g Sb-Eq) exhibits notably higher resource depletion compared to the OFB (9.1 g Sb-Eq) and VFB (8.4 g Sb-Eq). Periphery components, despite their limited weight (<1.7%), account for 88%, 80%, and 46% of the resource depletion of the VFB, OFB, and HFB, respectively. This is primarily caused by the production of inverters within the periphery subsystem, accounting for 84%, 77%, and 44% of the resource depletion of the VFB, OFB, and HFB, respectively. This is mainly due to the use of gold as a raw material for circuit production in the inverter.

Additionally, for the OFB, approximately 18% of the impact is caused by the production of energy subsystem, which is due to the production of constructions such as buildings and chemical plants used for producing the precursor chemicals. Materials such as copper and gold used as construction materials lead to high resource depletion. For the HFB, the energy subsystem (51%) has similar contribution as the periphery components. This can be attributed to the use of $ZnCl_2$ as both the negolyte active material and electrolyte additive in HFB, leading to a significantly higher metal resource depletion for the HFB compared to VFB and OFB.

3.1.6 Particulate matter formation. The HFB (8.5×10^{-6} disease incidence) exhibited the best particulate matter formation performance, followed by the OFB (1.6×10^{-5} disease incidence), and the VFB (3.1×10^{-5} disease incidence). For OFB, the production of MV emerges as the largest contributor, accounting for 54% of the particulate matter formation. This is primarily due to direct emissions (*i.e.*, ammonia, sulfur dioxide, and nitrogen oxides) from the MV production process (29%), as well as emissions from various upstream material production processes (25%). Another notable contributor is the production of posolyte material TEMPTMA (28%). This can be attributed to the use of methyl chloride (12%) as a raw material for precursor production, emissions from electricity production, as well as waste treatment processes. For the HFB, the posolyte active material TEMPO-4-SO_3K was the biggest contributor, accounting for 42% of the particulate matter formation. The production of end plates constitutes 18% of the total impact, primarily due to the use of aluminium collector foil. Peripheral components account for 15% of the particulate matter formation, with inverter production accounting for 13% and pump production contributing 2%. Additionally, $ZnCl_2$ production (10%) also contributes notably.

3.2 Cradle-to-use impacts

In addition to the impacts of battery production, the cradle-to-use impacts of the RFBs considers impacts caused during battery use phase, including the electrolyte replacements over the battery lifetime, as well as electricity loss. The electrolyte replacement frequency, the total energy delivered throughout the battery's lifespan and the amount of electricity loss in use phase are calculated by the battery performance model, and the results are presented in Table 5.

The impacts per kW h of energy delivered over the lifetime (FU2) is shown in Fig. 6(a). In most impact categories, the OFB demonstrates superior performance compared to the VFB, except for freshwater ecotoxicity. This is due to the high freshwater ecotoxicity associated with the OFB's electrolyte active material and a large amount of electrolyte consumed in the use phase. When comparing the LCA results with FU2 to FU1, the OFB exhibits better relative environmental performance among the studied RFBs. This can be attributed to its less frequent electrolyte replacements and the relatively higher lifetime energy delivered. In the comparison between FU2 and FU1 results for the HFB and VFB, the difference in environmental performance between the two batteries is enlarged across most impact categories. This is because electrolyte is the main contributor to the environmental impacts of battery production across various impact categories, with electrolyte replacement considered in the FU2 further amplifying these impacts. Therefore, it is not surprising to observe a substantial increase in the relative contribution of electrolyte active materials in the LCA results with FU2 compared to FU1, regardless of battery chemistries and impact categories. The electrolyte active materials account for 80 to 97% of the total impacts in FU2 in most impact categories except resource depletion. Consequently, the relative contribution of power subsystem and periphery subsystem is reduced, and the hotspots are otherwise similar to those described in section 3.1. However, the electricity loss in the use phase emerges as an additional main contributor, especially for resource depletion. This is because the studied RFBs are assumed to store electricity generated by rooftop photovoltaic systems, which require minerals like copper in their production processes.

Table 5 Electrolyte replacement frequency over the entire system lifetime and total energy delivered for the three RFBs

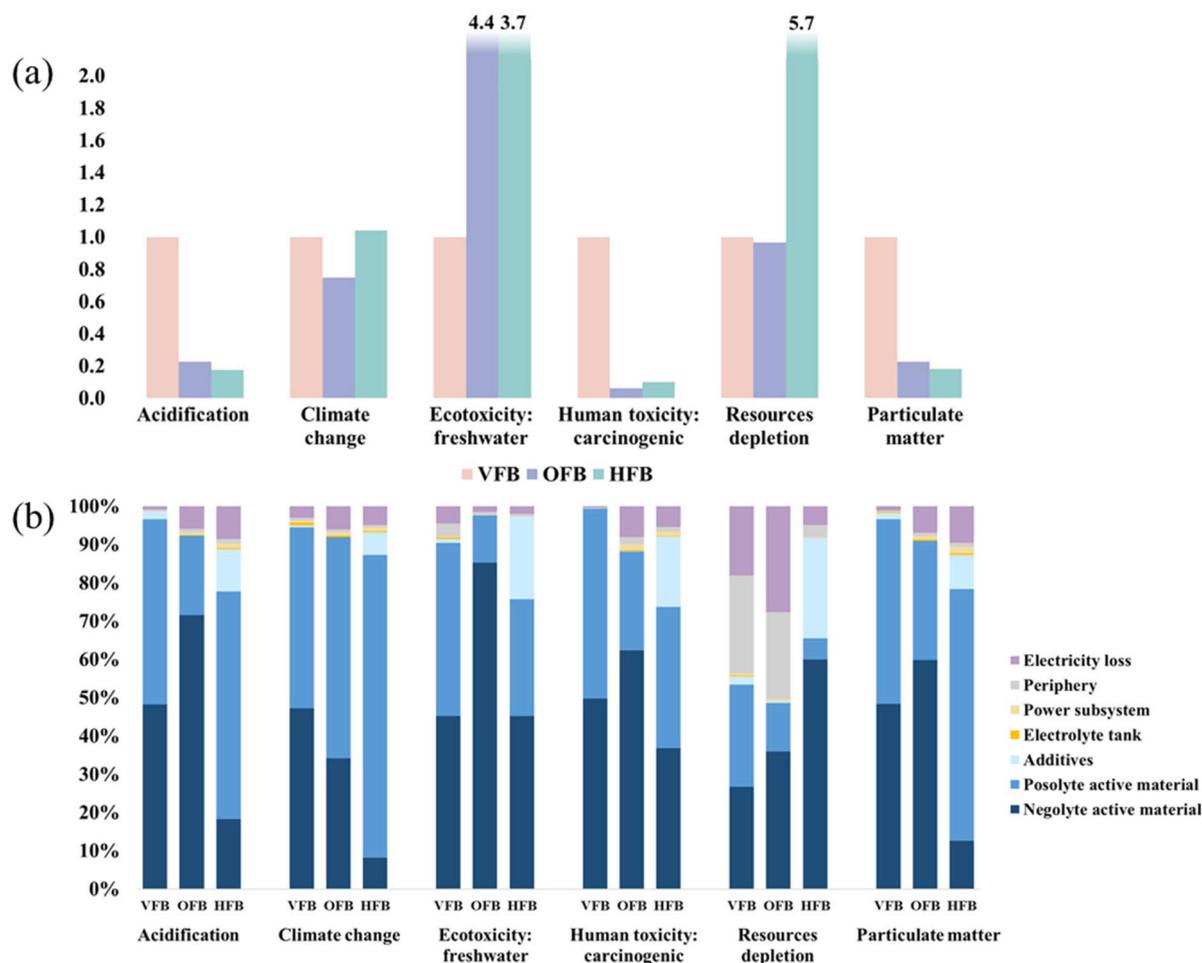|	VFB	OFB	HFB
Electrolyte replacement frequency (times)	18	9	22
Number of cycles the flow battery can perform before electrolyte replacement (cycles)	450	851	371
Total energy delivery (MW h)	157	185	196

Fig. 6 (a) Comparative environmental impacts of three RFBs, with a functional unit (FU2) of 1 kW h energy delivered over lifetime. The impacts of VRB are set to 1.0 for comparison. (b) Breakdown of environmental impacts from manufacturing three RFBs to battery components, with a FU of 1 kW h energy delivered over lifetime. VFB = vanadium flow battery, OFB = organic flow battery, HFB = hybrid flow battery.

3.3 Uncertainty analysis and sensitivity analysis

The results highlight CF as the predominant parameter contributing to the results uncertainty, regardless of battery chemistries and impact categories (Fig. 7). Moreover, the resource depletion results for the VFB also indicate significant contributions to uncertainty from other battery performance parameters.

4. Discussion

The lack of LCA studies on OFBs presents a challenge when searching for studies to compare with. Additionally, variations in FUs, LCIA methods, LCI databases, and assumptions regarding battery performance across previous studies make comparisons challenging. To ensure relevant comparisons, we converted all LCA results from previous studies to the same FU (per kW h energy storage, *i.e.* FU1), and converted our inventory to the same LCIA method used in the previous studies.

First, we compared our VFB results with previous studies to ensure our benchmark falls in a plausible value range. When

comparing to ref. 23, this study revealed results for acidification, climate impact, and human toxicity (carcinogenic) at 93%, 85%, and 73% of their findings, respectively. The disparities in these impact categories can be attributed to the updated background database used in our study. Furthermore, our comparison with[57] yielded findings at 84%, 91%, 84%, 114%, and 97% of their results for impact categories acidification, climate change, human toxicity (carcinogenic), resource depletion, and particulate matter, respectively. Discrepancies may stem from them having a global scope, whereas we focused on Europe.

Subsequently, we compared our OFB and HFB results with non-VFBs, using our VFB as benchmark, as shown in Fig. 8. The differences in environmental performance among different flow batteries can be attributed to two factors: the use of different materials, and variations in specific energy. The first factor determines the environmental impacts per unit of material, while the later factor determines the amount of materials required for the selected FU (per kW h energy capacity). Note that higher specific energy indicates less quantity of materials needed per FU.
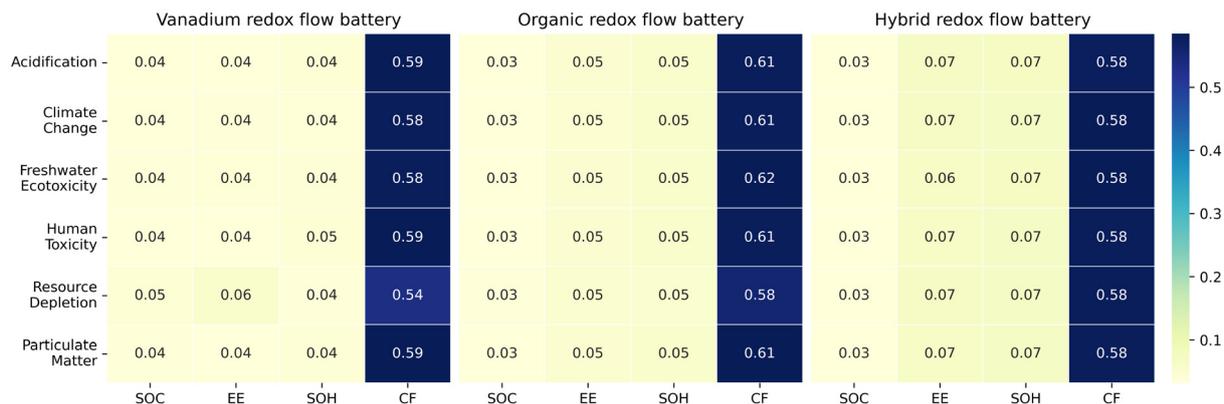
Fig. 7 Sensitivity analysis results with delta sensitivity index. The index values represent contributions to uncertainty in the impact scores, with 0 being the lowest (negligible) contribution.
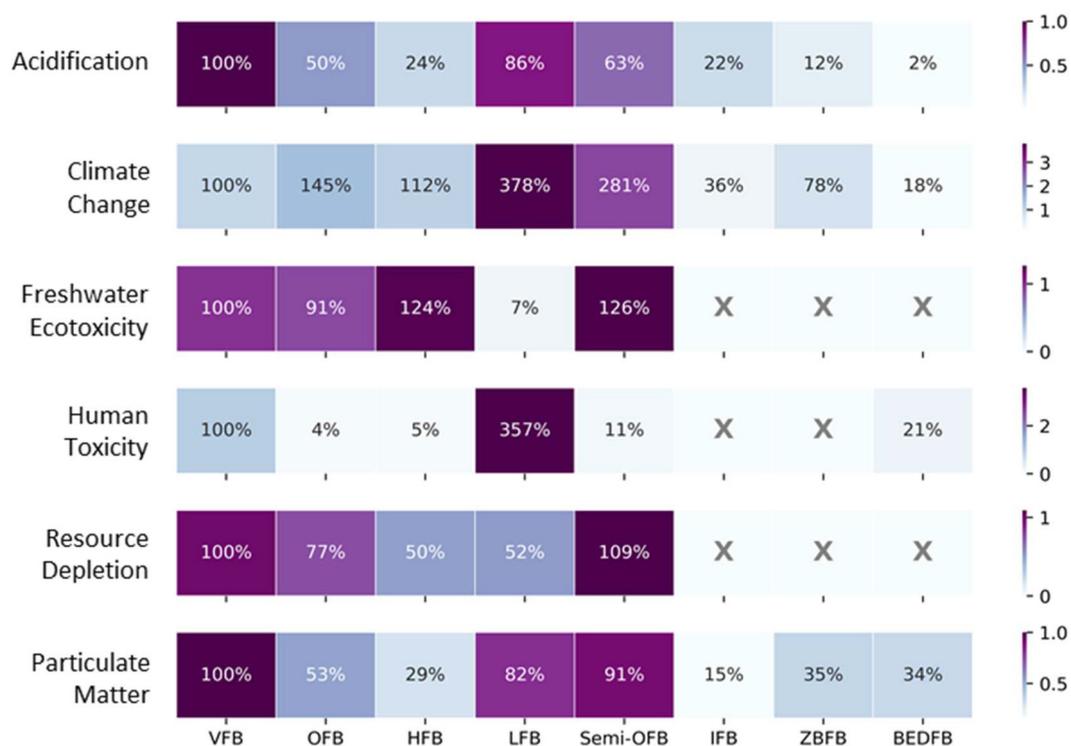

Fig. 8 Comparison with results from other studies. All results are converted to a functional unit of per kW h of energy capacity, using ReCiPe 2016 (H), then normalized based on the results of the VFB in this study for each impact categories. VFB = vanadium redox flow battery, OFB = organic redox flow battery, HFB = hybrid redox flow battery, LFB = lead redox flow battery, IFB = all-iron redox flow battery, ZBFB = zinc-bromine flow battery, BEDFB = bipolar electrodialysis flow battery. Inventory data are collected from ref. 58 (for LFB), ref. 26 (for semi-OFB), ref. 57 (for IFB and ZBFB), and ref. 37 (for BEDFB).

Compared to another semi-organic battery (semi-OFB) with anthraquinone-based electrolyte materials, our two RFBs with TEMPO-based electrolytes demonstrated lower impacts, despite the semi-OFB's slightly higher specific energy (18.72 W h kg^{-1} for semi-OFB vs. 16 and 15 W h kg^{-1} for OFB and HFB, respectively). However, when compared to all-iron redox flow batteries (IFBs) and zinc-bromine redox flow batteries (ZBFBs), our OFBs and HFBs generally exhibited higher impacts, except

for particulate matter, where the HFB had slightly lower impacts compared to the ZBFBs. This is due to the low environmental impacts associated to the production of electrolyte materials used in IFBs, and ZBFBs. In comparison to lead redox flow batteries (LFBs), HFBs and OFBs are outperformed across most impact categories, except for freshwater ecotoxicity and resource depletion. Notably, HFBs and OFBs showed the best performance among all batteries in the human toxicity (carcinogenic)

impact category. However, it is important to bear in mind the high uncertainty associated with toxicity-related impact methods.[59] BEDFBs performed best in acidification and climate impact among all batteries, although their human toxicity potential is 4–5 times higher than that of our RFBs.

It should to be noted that the absolute cradle-to-use (FU2) impacts of VFB are several times higher compared to previous studies.[23,57] This discrepancy arises from our assumption regarding electrolyte degradation, which previous studies did not consider, as they assumed no degradation during the use phase. By incorporating electrolyte degradation and replacement in the use phase, our study reveals substantially higher environmental impacts. This highlights the need for recirculating flow battery electrolytes and developing effective recycling methods.

SA results highlight the high influence of the CF on the uncertainty in the LCA results. The CF directly affects electrolyte replacement frequency and total energy delivery over the battery's lifespan. A lower CF rate implies less frequent electrolyte replacement throughout the battery's lifetime, thereby enhancing user experience and reducing environmental impacts associated with electrolyte production. This has particular importance for RFBs using electrolyte materials with high environmental impacts. This explains why the OFB exhibits improved environmental performance among studied batteries after considering battery performance in the LCA model. Despite its significance, the CF has often been excluded or assumed negligible in previous studies.[24,26,37] We recommend future studies to consider this parameter in LCA models of RFBs or, at minimum, in sensitivity analyses. Additionally, uncertainties in the emerging battery performance also indicate opportunities for improvement. Thus, the SA results also suggest that future research should prioritize improving electrolyte CF in order to reduce environmental impacts of both VFBs and RFBs with TEMPO-based electrolyte. In line with this, significant research effort have been dedicated to developing approaches for electrolyte stabilization.[60–63]

Several uncertainties and limitations exist in the study. First, this study excluded the EoL stage because the treatment of organic-based electrolytes is still under research.[16,64] While there are more mature EoL treatments for VFB electrolytes, such as replenishment or rebalancing, achieved through partial remixing of the posolyte and negolyte,[65,66] this method is applicable only to RFBs with similar active species in both electrolytes, such as vanadium for VFBs. For OFBs and HFBs with distinct (asymmetrical) active species in the negolyte and posolyte, suitable EoL treatments are still in early development and remain to be explored. In recent years, novel electrolyte rebalancing methods have been proposed for AQ-based RFBs,[64,67] however, there is a lack of method established for TEMPO-based RFBs. This exclusion may potentially influence comparative outcomes among batteries.[68] Further LCA studies are therefore recommended once relevant EoL technology for organic electrolytes has been developed. Another uncertainty lies in the use of current background databases to assess emerging technologies. One possible approach to address this issue is to use prospective LCA databases such as the ones generated by Premise. However, these databases primarily focus on future changes related to climate impacts.[69] Such inconsistency in databases pose challenges when assessing multiple environmental impacts as in this study. Additionally, while the toxicity impacts of battery components were assessed using available characterization factors from the EF method (USEtox model), certain active materials, particularly novel organic electrolytes, may not yet be fully represented in existing LCIA databases. As a result, the potential toxicity of the battery components themselves could be underestimated. This is an intrinsic limitation of the LCIA model. Furthermore, the choice of LCIA method affects battery environmental performance comparisons. Resource depletion and freshwater ecotoxicity methods from EF and ReCiPe 2016 (H) yield contrasting results, as results shown in Fig. 5(a) and 8. This is due to the intrinsic differences in the applied LCIA model approaches. For example, the EF method use the abiotic depletion potential (ultimate reserve) to measure the relative contribution of a product system to mineral resource depletion, whereas ReCiPe uses surplus ore potential to assess the relative consequences of a product system on changing mineral resource quality.[70]

5. Conclusion

Based on a functional unit of 1 kW h of storage capacity, this LCA study shows that both the OFB and HFB exhibit significantly better environmental performance in acidification, human toxicity (carcinogenic), and particulate matter compared to the VFB. While the OFB and HFB also show better environmental performance relative to anthraquinone-based semi-OFB across all impact categories, their performance varies across different impact categories when compared to other RFB chemistries. Key environmental hotspots in the battery production stage include the production of electrolyte active materials and inverter circuits. For the HFB, additional impacts stem from electrolyte additives and aluminum end plates. When the battery use phase is considered, the OFB outperforms both the HFB and VFB across most impact categories, largely due to its low electrolyte CF, which reduces the frequency of electrolyte replacement. Consequently, the environmental contribution of electrolyte active materials rises to 80–97% in most impact categories (except resource depletion) due to the increased impact of electrolyte replacement. Sensitivity analysis suggests that CF is the most significant contributor to total uncertainty among battery performance parameters, highlighting its potential for improving the environmental performance of both VFBs and TEMPO-based RFBs.

Abbreviations

VFB	Vanadium redox flow battery
PCS	Power conversion system
TMS	Thermal management system
OCV	Open circuit voltage

TAA	Total active area
N_c	Number of cells
AAC	Active area per cell
ΔSoC	Operating state-of-charge range
SoH	State of health
CF	Capacity fade
HDPE	High density polyethylene
V_2O_5	Vanadium pentoxide
H_2SO_4	Sulfuric acid
H_3PO_4	Phosphoric acid
RFBs	Redox flow batteries
TEMPTMA	N,N,N-2,2,6,6-Heptamethylpiperidin-4-ammonium chloride
TEMPO	2,2,6,6-Tetramethylpiperidine-1-oxyl
TEMPO-4-SO$_3$K	2,2,6,6-Tetramethylpiperidone-4-sulfate potassium
Intermediate 1	4-Dimethylamino-2,2,6,6-etramethylpiperidine
Intermediate 2	N,N,N-2,2,6,6-Heptamethylpiperidin-4-ammonium chloride
4-Hydroxy-TEMP	4-Hydroxy-2,2,6,6-tetramethylpiperidine
4-Hydroxy-TEMPO	4-Hydroxy-2,2,6,6-tetramethylpiperidine-N-oxyl
TAA	2,2,6,6-Tetramethyl-4-piperidone/triacetone amine.

Data availability

The data supporting this article have been included as part of the ESI.†

Conflicts of interest

There are no conflicts to declare.

Acknowledgements

References

1 Y. Abdelilah, H. Bahar, T. Criswell, P. Bojek, F. Briens, J. Moorhouse and L. M. Martinez, *Renewables 2022: Analysis and forecast to 2027*, Paris, 2023.

2 D. Bogdanov, J. Farfan, K. Sadovskaia, A. Aghahosseini, M. Child, A. Gulagi, A. S. Oyewo, L. D. N. S. Barbosa and C. Breyer, *Nat. Commun.*, 2019, **10**, 1–16.

3 Y. X. Yao, J. F. Lei, Y. Shi, F. Ai and Y. C. Lu, *Nat. Energy*, 2021, **6**, 582–588.

4 N. Nsitem., J. Chase and Y. Sekine. *Scaling the Residential Energy Storage Market*, BloombergNEF, 2023.

5 B. Chreim, M. Esseghir and L. Merghem-Boulahia, *Energy Rep.*, 2024, **11**, 250–260.

6 J. Figgener, P. Stenzel, K. P. Kairies, J. Linssen, D. Haberschusz, O. Wessels, G. Angenendt, M. Robinius, D. Stolten and D. U. Sauer, *J. Energy Storage*, 2020, **29**, 101153.

7 M. Park, J. Ryu, W. Wang and J. Cho, *Nat. Rev. Mater.*, 2017, **2**, 1–18.

8 C. C. Ye, A. Q. Wang, C. Breakwell, R. Tan, C. G. Bezzu, E. Hunter-Sellars, D. R. Williams, N. P. Brandon, P. A. A. Klusener, A. R. Kucernak, K. E. Jelfs, N. B. McKeown and Q. L. Song, *Nat. Commun.*, 2022, **13**, 3184.

9 T. Janoschka, N. Martin, U. Martin, C. Friebe, S. Morgenstern, H. Hiller, M. D. Hager and U. S. Schubert, *Nature*, 2015, **527**, 78–81.

10 T. B. Liu, X. L. Wei, Z. M. Nie, V. Sprenkle and W. Wang, *Adv. Energy Mater.*, 2016, **6**, 1501449.

11 K. E. Rodby, R. L. Jaffe, E. A. Olivetti and F. R. Brushett, *Int. J. Inf. Manage.*, 2023, **70**, 232605.

12 W. Wang, W. Xu, L. Cosimbescu, D. W. Choi, L. Y. Li and Z. G. Yang, *Chem. Commun.*, 2012, **48**, 6669–6671.

13 Z. N. Li, T. L. Jiang, M. Ali, C. X. Wu and W. Chen, *Energy Storage Mater.*, 2022, **50**, 105–138.

14 M. R. Gerhardt, L. C. Tong, R. Gómez-Bombarelli, Q. Chen, M. P. Marshak, C. J. Galvin, A. Aspuru-Guzik, R. G. Gordon and M. J. Aziz, *Adv. Energy Mater.*, 2017, **7**, 1601488.

15 B. Huskinson, M. P. Marshak, C. Suh, S. Er, M. R. Gerhardt, C. J. Galvin, X. D. Chen, A. Aspuru-Guzik, R. G. Gordon and M. J. Aziz, *Nature*, 2014, **505**, 195–198.

16 D. G. Kwabi, Y. L. Ji and M. J. Aziz, *Chem. Rev.*, 2020, **120**, 6467–6489.

17 S. J. Jin, Y. Jing, D. G. Kwabi, Y. L. Ji, L. C. Tong, D. De Porcellinis, M. A. Goulet, D. A. Pollack, R. G. Gordon and M. J. Aziz, *ACS Energy Lett.*, 2019, **4**, 1342–1348.

18 B. Hu, J. Luo, M. W. Hu, B. Yuan and T. L. Liu, *Angew. Chem., Int. Ed.*, 2019, **58**, 16629–16636.

19 T. Janoschka, N. Martin, M. D. Hager and U. S. Schubert, *Angew. Chem., Int. Ed.*, 2016, **55**, 14427–14430.

20 B. Hu, M. W. Hu, J. Luo and T. L. Liu, *Adv. Energy Mater.*, 2022, **12**, 2102577.

21 L. D. Lima, M. Quartier, A. Buchmayr, D. Sanjuan-Delmas, H. Laget, D. Corbisier, J. Mertens and J. Dewulf, *Sustainable Energy Technol.*, 2021, **46**, 101286.

22 N. Blume, M. Becker, T. Turek and C. Minke, *J. Ind. Ecol.*, 2022, **26**, 1796–1808.

23 S. Weber, J. F. Peters, M. Baumann and M. Weil, *Environ. Sci. Technol.*, 2018, **52**, 10864–10873.

24 J. Gouveia, E. Silva, T. Mata, A. Mendes, N. Caetano and A. Martins, *Energy Rep.*, 2020, **6**, 87–94.

25 M. Dieterle, P. Fischer, M. N. Pons, N. Blume, C. Minke and A. Bischi, *Sustainable Energy Technol.*, 2022, **53**, 102457.

26 G. Di Florio, I. Pucher, P. Todeschi, M. C. Baratto, R. Basosi and E. Busi, *J. Cleaner Prod.*, 2022, **343**, 130899.

27 G. Rodriguez-Garcia, H. C. Fu, P. Sullivan, C. J. Chen, Z. N. Song, J. Q. Chen, Y. F. Yan, D. W. Feng, S. Jin and I. Celik, *J. Cleaner Prod.*, 2023, **397**, 136533.

28 C. F. B. Rocha, Doctor Doctor thesis, Universiteit Leiden, 2022.

29 J. Winsberg, C. Stolze, A. Schwenke, S. Muench, M. D. Hager and U. S. Schubert, *ACS Energy Lett.*, 2017, **2**, 411–416.

30 J. Xiong, M. Jing, A. Tang, X. Fan, J. Liu and C. Yan, *J. Energy Storage*, 2018, **15**, 133–144.

31 R. Gundlapalli and S. Jayanti, *J. Energy Storage*, 2021, **33**, 102078.

32 M. Guarnieri, A. Trovò, A. D'Anzi and P. Alotto, *Appl. Energy*, 2018, **230**, 1425–1434.

33 Q. Xu, T. S. Zhao and P. K. Leung, *Appl. Energy*, 2013, **105**, 47–56.

34 J. Gouveia, A. Mendes, R. Monteiro, T. M. Mata, N. S. Caetano and A. A. Martins, *Energy Rep.*, 2020, **6**, 95–101.

35 Y. Hu, D. S. Soneira and M. J. Sánchez, *J. Energy Storage*, 2021, **35**, 102262.

36 M. Baumann, J. F. Peters, M. Weil and A. Grunwald, *Energy Technol.*, 2017, **5**, 1071–1083.

37 M. A. Morales-Mora, J. J. H. Pijpers, A. C. Antonio, J. D. Soto and A. M. A. Calderón, *J. Energy Storage*, 2021, **35**, 102339.

38 M. M. Rahman, A. O. Oni, E. Gemechu and A. Kumar, *Energy Convers. Manage.*, 2020, **223**, 113295.

39 S. Cucurachi, C. F. Blanco, B. Steubing and R. Heijungs, *J. Ind. Ecol.*, 2022, **26**, 374–391.

40 S. Wickerts, R. Arvidsson, A. Nordelöf, M. Svanström and P. Johansson, *ACS Sustainable Chem. Eng.*, 2023, **11**, 9553–9563.

41 R. Gross, R. Hanna, A. Gambhir, P. Heptonstall and J. Speirs, *Energy Policy*, 2018, **123**, 682–699.

42 C. Mutel, *et al.*, Brightway LCA Software Framework, **https://docs.brightway.dev/en/latest/**.

43 L. Tschümperlin, P. Stolz and R. Frischknecht, *Life cycle assessment of low power solar inverters*, 2016.

44 C. Capello, S. Hellweg, B. Badertscher and K. Hungerbuhler, *Environ. Sci. Technol.*, 2005, **39**, 5885–5892.

45 G. Geisler, T. B. Hofstetter and K. Hungerbuhler, *Int. J. Life Cycle Assess.*, 2004, **9**, 101–113.

46 F. Piccinno, R. Hischier, S. Seeger and C. Som, *J. Cleaner Prod.*, 2016, **135**, 1085–1097.

47 J. Niemeyer, M. Neumann, V. Brehme, M. Michel and C. Schwarz, EP2706056A1, 2012.

48 U. S. Schubert, T. Janoschka, N. Martin and M. Hager, *Worldwide Pat.*, 2016.

49 Z. Xiang, C. Zhang, X. Hu, J. Wang and B. Su, *China Pat*, CN115010650A, 2022.

50 S. D. Pastor, A. R. Smith and K. M. Bessonen, US5629426A, 1995.

51 J. Porzio and C. D. Scown, *Adv. Energy Mater.*, 2021, **11**, 21000771.

52 S. Ebner, S. Spirk, T. Stern and C. Mair-Bauernfeind, *ChemSusChem*, 2023, **16**, e202201818.

53 E. Borgonovo, *Reliab. Eng. Syst. Saf.*, 2007, **92**, 771–784.

54 E. Plischke, E. Borgonovo and C. L. Smith, *Eur. J. Oper. Res.*, 2013, **226**, 536–550.

55 T. Iwanaga, W. Usher and J. Herman, *Socio-Environ. Syst. Modell.*, 2022, **4**, 18155–18155.

56 A. Saltelli, M. Ratto, T. Andres, F. Campolongo, J. Cariboni, D. Gatelli, M. Saisana and S. Tarantola, *Global sensitivity analysis: the primer*, John Wiley & Sons, 2008.

57 H. Y. He, S. Tian, B. Tarroja, O. A. Ogunseitan, S. Samuelsen and J. M. Schoenung, *J. Cleaner Prod.*, 2020, **269**, 121740.

58 E. Shittu, R. Suman, M. K. Ravikumar, A. K. Shukla, G. L. Zhao, S. Patil and J. Baker, *J. Cleaner Prod.*, 2022, **337**, 130503.

59 R. K. Rosenbaum, T. M. Bachmann, L. S. Gold, M. A. J. Huijbregts, O. Jolliet, R. Juraske, A. Koehler, H. F. Larsen, M. MacLeod, M. Margni, T. E. McKone, J. Payet, M. Schuhmacher, D. van de Meent and M. Z. Hauschild, *Int. J. Life Cycle Assess.*, 2008, **13**, 532–546.

60 W. J. Li, S. W. Liao, Z. P. Xiang, M. B. Huang, Z. Y. Fu, L. B. Li and Z. X. Liang, *Chem. Eng. Sci.*, 2023, **270**, 118534.

61 G. G. Tang, W. Y. Wu, Y. H. Liu, K. Peng, P. P. Zuo, Z. J. Yang and T. W. Xu, *Nat. Commun.*, 2025, **16**, 47.

62 M. B. Huang, W. J. Li, D. H. Lin, K. Wan, Z. Y. Fu, Z. P. Xiang and Z. X. Liang, *Energy Storage Mater.*, 2024, **67**, 103267.

63 Y. F. Liu, X. Z. Yuan, M. B. Huang, Z. P. Xiang, S. Z. Hu, Z. Y. Fu, X. H. Guo and Z. X. Liang, *Ind. Eng. Chem. Res.*, 2022, **61**, 14508–14514.

64 Y. Jing, E. W. Zhao, M. A. Goulet, M. Bahari, E. M. Fell, S. J. Jin, A. Davoodi, E. Jónsson, M. Wu, C. P. Grey, R. G. Gordon and M. J. Aziz, *Nat. Chem.*, 2022, **14**, 1103–1109.

65 M. Skyllas-Kazacos and M. Kazacos, *J. Power Sources*, 2011, **196**, 8822–8827.

66 A. Bhattarai, P. C. Ghimire, A. Whitehead, R. Schweiss, G. G. Scherer, N. Wai and H. H. Hng, *Batteries*, 2018, **4**, 48.

67 M. Cantera, L. Lubián, K. Cavusoglu, R. Rubio-Presa, R. Sanz, V. Ruiz, J. M. Cámara and E. Ventosa, *Batteries Supercaps*, 2024, **7**, e202400086.

68 N. Blume, O. Zielinski, M. Becker and C. Minke, *Energy Technol.*, 2023, 2300750.

69 B. Steubing, A. M. Beltran and R. Sacchi, *Int. J. Life Cycle Assess.*, 2023, **28**, 1092–1103.

70 M. A. J. Huijbregts, Z. J. N. Steinmann, P. M. F. Elshout, G. Stam, F. Verones, M. Vieira, M. Zijp, A. Hollander and R. van Zelm, *Int. J. Life Cycle Assess.*, 2017, **22**, 138–147.